Theoretical Study of the Nonlinear Optical Properties of $KTiOPO_4$: Effects of Ti--O--Ti Bond Angles and Oxygen Electronegativity

M. Munowitz* and R. H. Jarman

Amoco Technology Company, P.O. Box 3011, Naperville, Illinois 60566-7011

J. F. Harrison

Department of Chemistry and Center for Fundamental Materials Research, Michigan State University, East Lansing, Michigan 48824-1322

Received May 5, 1993. Revised Manuscript Received June 29, 1993®

Second harmonic generation in the model system $[TiO_5\text{--}TiO_6\text{--}TiO_5]^{20-}$ is studied using a perturbative sum-over-states formalism together with extended Hückel wave functions. The nonlinear response of the central TiO_6 group, a distorted octahedron with its fourfold axis defined by the atoms O1--Ti--O2, improves both with increasing Ti--O--Ti angle and with decreasing electronegativity of the chain oxygens. A small shift of charge toward the distant oxygen, O1, takes place as the Ti--O--Ti angle is increased, thereby enlarging the electronic third moment and with it the local hyperpolarizability. Reducing the electronegativity of the oxygens, by contrast, brings about a near-resonant enhancement of the hyperpolarizability, which occurs as energies of the highest occupied molecular orbitals are raised. These results are placed in the context of recent experimental measurements involving compounds isomorphic to $KTiOPO_4$.

Introduction

This paper is part of a series describing second harmonic generation in certain model systems representative of potassium titanyl phosphate ($KTiOPO_4$, or KTP).[1-4] Well-known for its nonlinear optical response at infrared frequencies,[5-9] KTP is also the principal member of a growing family of chemically substituted isomorphs.[10-23] Nonlinear optical properties vary widely among these related materials (surprisingly, perhaps, in view of what sometimes seem to be only subtle structural differences), and a consistent theoretical understanding of any common mechanism clearly would be beneficial. The present work offers a limited, but systematic, assessment of how variations in Ti--O--Ti angle and oxygen electronegativity affect the nonresonant hyperpolarizability computed for an idealized chain of three interconnected TiO_6 octahedra. This study draws upon the results and assumptions of the two most recent reports in the series.[3,4]

Crystalline KTP, the parent structure, contains chains of TiO_6 octahedra alternating with PO_4 tetrahedra parallel to the *a* and *b* axes of an orthorhombic unit cell.[24] The TiO_6 groups themselves form helices in which the octahedra are linked alternately cis and trans, and the potassium ions occupy channels running through the framework parallel to the *a* and *c* axes. There are, in addition, two crystallographic sites for each of K, Ti, and P. Figure 1 provides two views of the overall crystal structure.

Substitution is possible at any of the K, Ti, or P positions in the crystal. Some of the known isomorphic systems referred to above include those where (1) K is replaced by Na, Rb, Cs, Tl, Ag, or NH_4, (2) Ti is replaced by Sn and Sb, and (3) P is replaced by As. As stated above, nonlinear optical properties exhibit considerable variation among these materials. Substitution of arsenic for phosphorus to yield $KTiOAsO_4$, for example, seems to enhance second harmonic generation by up to approximately 15%.[13,18]

* Abstract published in *Advance ACS Abstracts*, September 1, 1993.

(1) Jarman, R. H.; Munowitz, M.; Harrison, J. F. *J. Cryst. Growth* **1991**, *109*, 353.
(2) Munowitz, M.; Jarman, R. H.; Harrison, J. F. *J. Phys. Chem.* **1992**, *96*, 124.
(3) Munowitz, M.; Jarman, R. H.; Harrison, J. F. *Chem. Mater.* **1992**, *4*, 1296.
(4) Munowitz, M.; Jarman, R. H.; Harrison, J. F. *Chem. Mater.* **1993**, *5*, 661.
(5) Zumsteg, F. C.; Bierlein, J. D.; Gier, T. E. *J. Appl. Phys.* **1976**, *47*, 4980.
(6) Eimerl, D. *Proc. SPIE-Int. Soc. Opt. Eng.* **1986**, *681*, 5.
(7) Fan, T. Y.; Huang, C. E.; Hu, B. Q.; Eckhardt, R. C.; Fan, Y. X.; Byer, R. L.; Feigelson, R. S. *Appl. Opt.* **1987**, *26*, 2391.
(8) Vanherzeele, H.; Bierlein, J. D.; Zumsteg, F. C. *Appl. Opt.* **1988**, *27*, 3314.
(9) (a) Baumert, J. C.; Schellenberg, F. M.; Lenth, W.; Risk, W. P.; Bjorklund, G. C. *Appl. Phys. Lett.* **1987**, *51*, 2192. (b) Risk, W. P.; Baumert, J. C.; Bjorklund, G. C.; Schellenberg, F. M.; Lenth, W. *Appl. Phys. Lett.* **1988**, *52*, 85.
(10) Jarman, R. H.; Grubb, S. G. *Proc. SPIE Conf. Ceram. Inorg. Cryst Opt. Electroopt. Conv.* **1988**, *968*, 108.
(11) Crennell, S. J.; Owen, J. J.; Grey, C. P.; Cheetham, A. K.; Kaduk, J. A.; Jarman, R. H. *J. Mater. Chem.* **1991**, *1*, 113.
(12) Crennell, S. J.; Morris, R. E.; Cheetham, A. K.; Jarman, R. H. *Chem. Mater.* **1992**, *4*, 82.
(13) Crennell, S. J.; Cheetham, A. K.; Jarman, R. H.; Thrash, R. J.; Kaduk, J. A. *J. Mater. Chem.* **1992**, *2*, 383.
(14) Crennell, S. J.; Cheetham, A. K.; Kaduk, J. A.; Jarman, R. H.; *J. Mater. Chem.* **1992**, *2*, 785.
(15) Stucky, G. D.; Phillips, M. L. F.; Gier, T. E. *Chem. Mater.* **1989**, *1*, 492.
(16) Phillips, M. L. F.; Harrison, W. T. A.; Gier, T. E.; Stucky, G. D.; *Proc. SPIE-Int. Soc. Opt. Eng.* **1989**, *1104*, 225.
(17) Phillips, M. L. F.; Harrison, W. T. A.; Gier, T. E.; Stucky, G. D.; Kulkarni, G. V.; Burdett, J. K. *Inorg. Chem.* **1990**, *29*, 2158.
(18) Phillips, M. L. F.; Harrison, W. T. A.; Stucky, G. D.; McCarron, E. M.; Calabrese, J. C.; Gier, T. E. *Chem. Mater.* **1992**, *4*, 222.
(19) Marnier, G.; Boulanger, B.; Manaert. *J. Phys.: Condens. Matter* **1989**, *1*, 5509.
(20) El Haidouri, A.; Durand, J.; Cot, L. *Mater. Res. Bull.* **1990**, *25*, 1193.
(21) Crosnier, M. P.; Guyomard, D.; Verbaere, A.; Piffard, Y. *Eur. J. Solid State Inorg. Chem.* **1990**, *27*, 845.
(22) Thomas, P. A.; Mayo, S. C.; Watts, B. E. *Acta Crystallogr.* **1992**, *B48*, 401.
(23) Ravez, J.; Simon, A.; Boulanger, B; Crosnier, M. P.; Piffard, Y. *Ferroelectrics* **1991**, *124*, 379.
(24) Tordjman, I.; Masse, R.; Guitel, J. C. *Z. Kristallogr.* **1974**, *139*, 103.

0897-4756/93/2805-1257$04.00/0

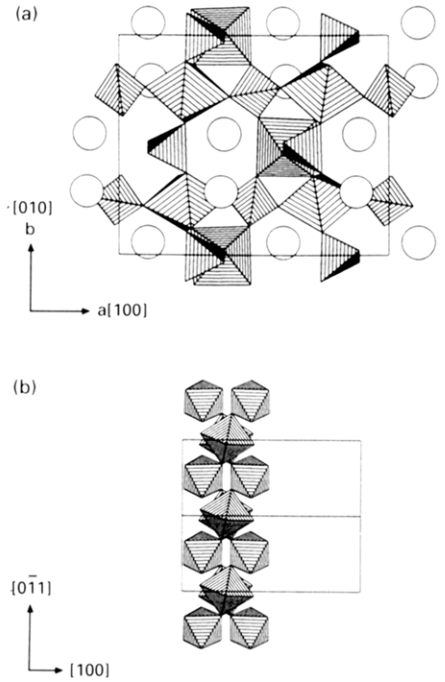

Figure 1. Structure of the KTP crystal. (a) A projection along [001], showing alternating TiO_6 octahedra and PO_4 tetrahedra. The potassium sites are indicated by open circles. (b) A view along [011], illustrating two intertwined chains of octahedra. One oxygen atom is shared by each pair of octahedra.

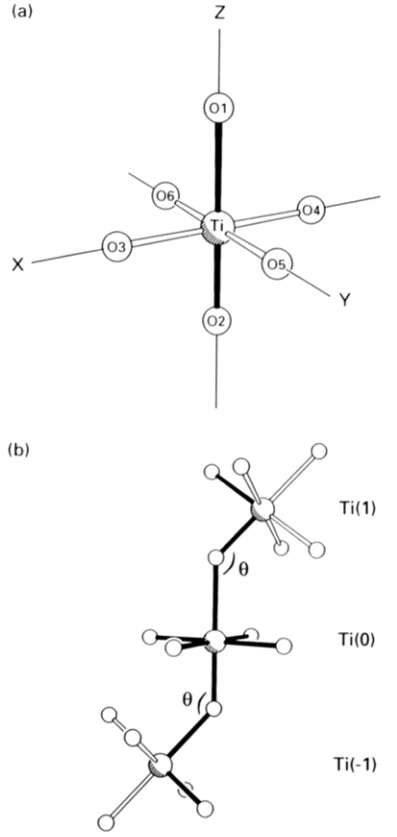

Figure 2. Idealized representation of the TiO_6 chains in KTP. (a) The coordinate system is defined relative to the TiO_6 subunit at the center of the chain. This central grouping is distorted along a C_4 axis (z), with O1 and O2 denoting, respectively, the distant and near oxygens. Long Ti--O bonds are fixed at 2.15 Å, short Ti--O bonds at 1.74 Å, and intermediate Ti--O bonds at 1.99 Å. (b) Trimer: bonds in the central TiO_6 group and along the O--Ti--O--Ti--O--Ti--O chain are rendered in solid black. The numbers associated with the titanium atoms (1, 0, −1) label the individual TiO_6 groups in the chain, and θ denotes the Ti--O--Ti angles. Groups 1 and −1 are linked to the central unit, group 0, via axial oxygens O1 and O2.

Replacement of titanium by tin, however, leads to a marked degradation in performance,[10] whereas results are mixed for cation substitution. Various arguments, often based on chemical intuition, have been made to account for the data, but there seems to have been little in the way of calculation or detailed justification.

Common to all these structures is a characteristic --Ti--O--Ti--O-- chain which is formed by the sharing of oxygens between adjacent TiO_6 groups. The Ti--O distances in the backbone of KTP follow a pattern of long (~2.10 Å), intermediate (~1.96 Å), and short (~1.74 Å) contacts, with the entire chain derived from a root octahedron distorted along a 4-fold axis (Figure 2a). Our previous work has addressed both the behavior of just an isolated TiO_6 group[3] and also the local response of TiO_6 when it is embedded in a chain of octahedra as in the actual crystal (Figure 2b).[4] For the TiO_6 group alone, we have examined how the hyperpolarizability tensor β responds to variations in the long and short Ti--O distances; for the chains (with fixed Ti--O--Ti angles), we have noted a similar dependence on the Ti--O contacts as well as an overall enhancement of the hyperpolarizability. Yet what varies most among the isomorphs of KTP are not the internuclear distances but rather the interconnection angles and the electronic environment external to the --Ti--O--Ti--O chains. The basic structure of the TiO_6 group is largely conserved in the different materials. Accordingly, we now consider the changes in β effected by varying the Ti--O--Ti angle and by perturbing the original electron distribution.

As before, the approach will be qualitative and aimed solely at identifying relationships and trends within a carefully controlled family of model systems. We use for this purpose a perturbative sum-over-states formalism[25-27] combined with extended Hückel wave functions,[28] arguingthat relative values within the series should be preserved while acknowledging the almost certain error of any individual value. Notwithstanding the well-recognized limitations of a one-electron model, the extended Hückel approach offers a number of advantages for a study of this type. First, the simplicity of the calculation makes it possible to examine a wide range of structures within a consistent framework. Second, both the symmetry of the molecular orbitals and gross features of the electron distribution should be maintained despite the simplifying approximations. Third, the singly-excited states are generated merely by promotion of an electron from an occupied to a virtual orbital, so that the single determinant thus created is actually an exact solution given the assumptions of the model. Fourth, and particularly interesting for the present study, the electron distribution can be easily manipulated just by altering the orbital parameters (essentially the atomic ionization potentials). We use this possibility here to simulate the effects of

(25) Armstrong, J. A.; Bloembergen, N.; Ducuing, J.; Pershan, P. S. *Phys. Rev.* **1962**, *127*, 1918.
(26) (a) Ward, J. F. *Rev. Mod. Phys.* **1965**, *37*, 1. (b) Orr, J. B.; Ward, J. F. *Mol. Phys.* **1971**, *20*, 513.
(27) Pugh, D.; Morley, J. O. In *Nonlinear Optical Properties of Organic Molecules and Crystals*; Chemla, D. S., Zyss, J., Eds.; Academic Press: Orlando, FL, 1987; Vol. 1, pp 193–225.
(28) (a) Hoffmann, R. *J. Chem. Phys.* **1963**, *39*, 1397. (b) Janiak, C.; Hoffmann, R. *J. Am. Chem. Soc.* **1990**, *112*, 5924.

certain cations on the electronegativity of the chain oxygens.

The simplicity of a Hückel calculation is instructive in itself since, naive as this method is, the model is still more sophisticated than much of the reasoning used so far to predict structure–function relationships among the KTP isomorphs. Recognition that KTP is a highly complex solid-state system has, from the beginning, created the understandable temptation to explain its nonlinear optical properties in the simplest terms possible. Popular approaches have included two-level and three-level models, which often focus on fragments as small as a single Ti--O group and which may use simplified bond–charge pictures for the hyperpolarizability.[29-32] In working at the current level of approximation, though, we demonstrate that such methods become increasingly difficult to justify. The results of the extended Hückel calculations, while not quantitatively correct, show nevertheless that it is unrealistic to ascribe the nonlinear optical properties to just one or two virtual transitions of either a TiO or a TiO_2 or a TiO_6 group.[3,4] Numerous matrix elements contribute to the perturbative expression for β, and the net value frequently arises as the result of near cancellation by large, opposing contributions. Neither concentrating on one transition nor examining the dipole moment of one excited state will suffice to model the phenomena completely; moreover, simple pictures appropriate for isolated fragments may be inadequate for understanding the cooperative nonlinear response of highly delocalized systems such as KTP.[4] Yet another caution is the demonstrated sensitivity of β to even very small perturbations of the electron density, as will become clear below.

It is with such considerations in mind that we have undertaken the present study. The goals here are to identify basic patterns in the nonlinear response and especially to estimate the magnitude and direction of the changes. The background provided by this model should be useful both for assessing various explanations of nonlinear optical behavior and for permitting a comparison with subsequent, more sophisticated calculations.

Formalism

Tensors. The first hyperpolarizability tensor, β, is defined through the expression

$$p_i = \alpha_{ij}(\omega)\, E_j(\omega) + \beta_{ijk}(-\omega;\omega_1, \omega_2)\, E_j(\omega_1)E_k(\omega_2) + \gamma_{ijkl}(-\omega;\omega_1',\omega_2',\omega_3')\, E_j(\omega_1')\, E_k(\omega_2')\, E_l(\omega_3') + \ldots \quad (1)$$

where p_i ($i = x, y, z$) is a component of the dipole moment induced in the molecule by time dependent electric fields $E(\omega)$. Repeated indexes are understood to be summed over the three Cartesian coordinates.

Under second harmonic generation (SHG), an incident field oscillating at angular frequency ω induces a dipole moment oscillating at 2ω. According to Kurtz and Perry,[33] the intensity measured in a powder sample (for unpolarized fundamental and second harmonic) is then proportional to the angular averages of the squared hyperpolarizability components, $\langle\beta^2\rangle$. Expressions for $\langle\beta^2\rangle$ specifically used in this paper are collected in the Appendix, while we refer to Cyvin et al.[34] for details of their derivation.

Sum over States. For SHG, the standard perturbative expression for β_{ijk} involves excited-state energies and dipole transition moments.[25-27] Individual components of the SHG tensor are expressed as

$$\beta_{ijk}(-2\omega;\omega,\omega) = -(e^3/8\hbar^2)\sum_{n,m} 2\{(\langle ijk\rangle + \langle ikj\rangle)[f(2\omega,\omega) + f(-2\omega,-\omega)] + (\langle kij\rangle + \langle jik\rangle)f(\omega,-\omega)\} \quad (2)$$

where each quantity

$$\langle ijk\rangle = \langle g|\hat{R}_i|n\rangle\langle n|\hat{R}_j|m\rangle\langle m|\hat{R}_k|g\rangle \quad (3)$$

involves transition moments between two excited states, $|m\rangle$ and $|n\rangle$, and the ground state $|g\rangle$. The dipole moments are referred to particular axes as denoted by the N-electron position operator $\hat{R}_i$ ($=\hat{X}, \hat{Y}, \hat{Z}$). Factors

$$f(2\omega,\omega) = [(\omega_n + 2\omega)(\omega_m + \omega)]^{-1} \quad (4a)$$

$$f(-2\omega,-\omega) = [(\omega_n - 2\omega)(\omega_m - \omega)]^{-1} \quad (4b)$$

$$f(\omega,-\omega) = [(\omega_n + \omega)(\omega_m - \omega)]^{-1} \quad (4c)$$

in which ω_n is the energy difference (in units of angular frequency) between $|n\rangle$ and $|g\rangle$, relate the energies of the incident and doubled light to that of the excited states. These expressions are only valid far away from all resonances, although phenomenological damping terms $i\Gamma_{ng}$ and $i\Gamma_{mg}$ can be added to the denominators in order to remove any singularities.

A very rough estimate of the hyperpolarizability is afforded by the Unsöld approximation, under which the sum over excited states may be collapsed to a single, ground-state expectation value.[35] The principal assumption is that the energy factors f are largely constant in the various excited states and hence may be taken outside the summation and incorporated (as some average value) into a constant K outside. The expression that remains is thereby reduced to

$$\tilde{\beta}_{ijk} = K\sum_{n,m}\langle g|\hat{R}_i|n\rangle\langle n|\hat{R}_j|m\rangle\langle m|\hat{R}_k|g\rangle \quad (5)$$

which, in a coordinate system where the ground-state dipole moment $\langle g|\hat{R}|g\rangle$ is zero, is evaluated exactly as

$$\tilde{\beta}_{ijk} = K\langle g|\hat{R}_i\hat{R}_j\hat{R}_k|g\rangle \quad (6)$$

To the extent that variation in the factors f can be ignored, the hyperpolarizability components thus become proportional to the ground-state expectation values of the electronic third moments.

Further details of the sum-over-states formalism, including a description of its implementation using LCAO-MO wave functions, are available in a previous paper.[3]

Extended Hückel Theory. Briefly, we recall that the Hückel model uses a one-electron Hamiltonian with diagonal elements H_{ii} specified by parameters. Values of

(29) Phillips, J. C.; van Vechten, J. A. *Phys. Rev.* **1969**, *183*, 709.
(30) (a) Levine, B. F. *Phys. Rev. Lett.* **1969**, *22*, 787. (b) Levine, B. F. *Phys. Rev. Lett.* **1970**, *25*, 440. (c) Levine, B. F. *Phys. Rev. B* **1973**, *7*, 2591. (d) Levine, B. F. *Phys. Rev. B* **1973**, *7*, 2600. (e) Levine, B. F. *Phys. Rev. B* **1974**, *10*, 1655.
(31) (a) Bergman, J. G.; Crane, G. R. *J. Chem. Phys.* **1974**, *60*, 2470. (b) Tofield, B. C.; Crane, G. R.; Bergman, J. G. *J. Chem. Soc., Trans. Faraday Soc.* **1974**, 1488. (c) Bergman, J. G.; Crane, G. R. *J. Solid State Chem.* **1975**, *12*, 172.
(32) Hansen, N. K.; Protas, J.; Marnier, G. *C. R. Acad. Sci. Paris, Ser. II* **1988**, *307*, 475.
(33) Kurtz, S. K.; Perry, T. T. *J. Appl. Phys.* **1968**, *39*, 3798.
(34) Cyvin, S. J.; Rauch, J. E.; Decius, J. C. *J. Chem. Phys.* **1965**, *43*, 4083.
(35) Unsöld, A. *Z. Phys.* **1927**, *43*, 563.

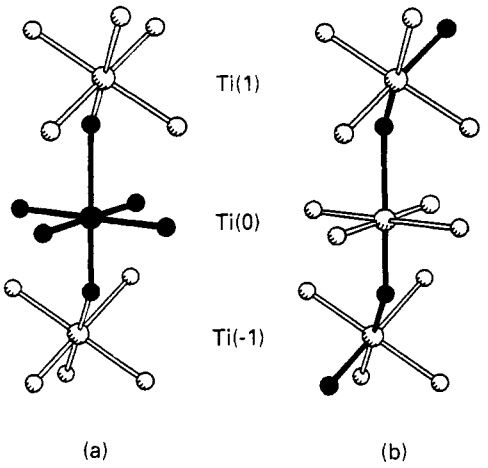

Figure 3. (a) Local hyperpolarizabilities may be computed for just the central TiO_6 group, taken as a fully integrated subsystem within the trimer. This titanium and its six-coordinated oxygens (solid black) remain stationary throughout. (b) In subsequent analysis, the effective ionization potentials of the chain oxygens (black) are deliberately varied. Local hyperpolarizabilities are then computed for the monomer depicted in panel (a).

H_{ii} typically correspond to ionization energies of the various atomic orbitals ϕ_i. In extended Hückel theory[28] the off-diagonal elements H_{ij} are proportional to the overlap integrals S_{ij}, being estimated as $-1.75S_{ij}(H_{ii}H_{jj})^{1/2}$. Additional information concerning the calculation is again provided in earlier work, where values of all parameters are tabulated.[3] For present purposes we note that the standard value of H_{ii} for the oxygen 2p orbital is −14.8 eV.

Computational Model

Structure. A system of three TiO_6 groups is the minimum necessary both to explore the effect of the Ti--O--Ti angle and to capture something of the properties of the extended chain. The model structure is built from the distorted TiO_6 octahedron illustrated in Figure 2a, with the axial oxygens (O1 and O2) of the central TiO_6 group serving as bridging atoms to the upper and lower units as shown in Figure 2b. Ti--O bond distances of 2.15, 1.74, and 1.99 Å are used, respectively, for the long (O1), short (O2), and intermediate (O3, O4, O5, O6) positions in the central octahedron, and the entire cluster thus generated is formally viewed as arising from Ti^{4+} and O^{2-} species[36] to yield $[TiO_5\text{-}TiO_6\text{--}TiO_5]^{20-}$. The upper and lower TiO_6 groups are positioned by means of the coordinate rotations and translations described in ref 4, for which purpose we regard a Ti--O--Ti bond angle of 135° as typical of the actual KTP system. The internuclear distances stated above have similarly been chosen to represent an average crystal structure in the family of isomorphs.

Local Hyperpolarizability. Our analysis will pertain exclusively to the *local* nonlinear response of the central TiO_6 alone, viewed within the context of the larger chain.[4] We compute, specifically, the microscopic hyperpolarizability originating from just the seven atoms of the central unit, using only those portions of the molecular orbitals with amplitude at the relevant positions. Computation of the local β for this subsystem (shown shaded in Figure 3a) involves first expressing the molecular orbitals for the complete chain as a linear combination of atomic orbitals at all positions, from which a normalized and antisymmetric wave function is formed in the usual way. For subsequent evaluations of the matrix elements in (3), the molecular orbital expansions are then truncated to include only those atomic orbitals within the desired subset. The overall electronic structure is therefore not disturbed in any way, but local attributes such as population density and dipole transition moments are obtained free of edge effects from the terminal oxygens. Moreover, since the atoms of the central TiO_6 never move, local hyperpolarizabilities for structures with different Ti--O--Ti angles may be compared on a consistent basis. Changes in the tensor elements attributable solely to coordinate rotations do not appear in this model, so any variation of the local β is a pure electronic effect and not simply the geometric consequence of a tensor transformation.

The two Ti--O--Ti angles, designated θ in Figure 2b, are taken as equal and then varied from 125° to 145° in the present study. For variation of the Hückel parameters H_{ii}, we distinguish the four backbone oxygens (shown shaded in Figure 3b) from those outside the --Ti--O--Ti--O-- chain. The local hyperpolarizability of just the central TiO_6 group similarly reflects the altered electronic distribution of the entire system.

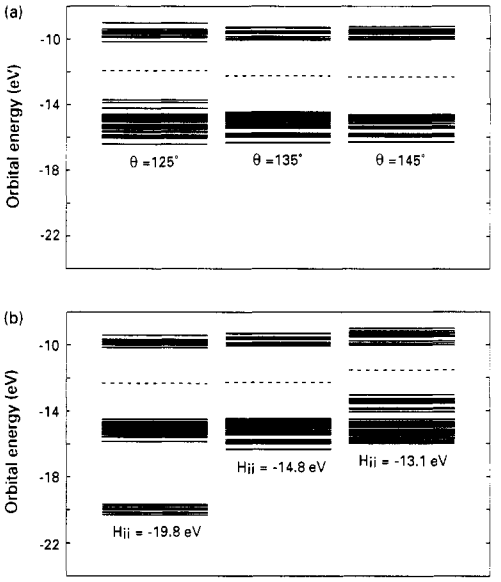

Figure 4. Highest occupied and lowest unoccupied energy levels, as predicted by extended Hückel theory. Midpoints between HOMO and LUMO are indicated by the broken lines. (a) Structures with various Ti--O--Ti angles but standard values of H_{ii}. (b) Effects of different values of H_{ii}; θ = 135°. Of the 91 eigenvectors that emerge from the molecular orbital calculation, a subset consisting of numbers 17 through 73 (see text) is shown here and used in each case for all computations of β.

Energy Levels and Molecular Orbitals

There are 91 molecular orbitals available to $[TiO_5\text{--}TiO_6\text{--}TiO_5]^{20-}$, of which the lowest 64 are occupied. Shown in Figure 4a is a subset of energy levels used in the calculation of β, for each of three systems with θ = 125°, 135°, and 145° (and standard values of H_{ii}). These orbitals, numbered 17–73, may be classified roughly according to the mixture of titanium and axial oxygen functions in the TiO_6 groups: (1) d–p π and σ bonding combinations (orbitals 17–30), (2) various π and σ nonbonding arrangements that exclude the central titanium (orbitals 31–64),

(36) Hansen, N. K.; Protas, J.; Marnier, G. *Acta Crystallogr.* **1991**, *B47*, 660.

and (3) the principal d–p π^* and σ^* antibonding orbitals (numbers 65–73).[3,4] The gap between the highest occupied and lowest unoccupied molecular orbital (HOMO – LUMO) is 4.4 eV at $\theta = 135°$, which may be compared to an experimentally measured absorption edge of 3.54 eV.[5]

Below the bonding orbitals lie mostly unmixed atomic core functions (molecular orbitals 1–16), while above the antibonding orbitals shown in the diagram are additional out-of-phase combinations and various other mixtures involving titanium p and d functions (orbitals 74–91). We consistently exclude these two outlying groups of levels from the calculation of β, accepting a small systematic error in return for a simplified computation. The spectroscopically favorable levels (17–73) account for 90–95% of the value of β in the sum-over-states calculation.

Despite some differences in composition and energy, the molecular orbitals maintain a relatively consistent pattern as θ is increased from 125° to 145°. Changes in the Hückel parameters for the chain oxygens, however, lead to more dramatic shifts, as is illustrated in Figure 4b. Across the three panels here, H_{ii} for the four relevant oxygens (Figure 3b) is taken as −19.8 eV, −14.8 eV (standard), and −13.1 eV in a structure with a fixed Ti--O--Ti angle of 135°. Making H_{ii} very negative (−19.8 eV) increases the electronegativity of O1 and O2 to the point where these atoms withdraw charge from titanium almost completely. As a result, orbitals 17–28 shift downward by about 5 eV and become effectively localized. Molecular orbitals in this group are largely combinations of various p functions from the chain oxygens, with most of the additional electron density coming from the depletion of the titanium d_{xz} and d_{yz} atomic orbitals. A typical distribution of electron density in such an orbital is provided in Figure 5a. At the other extreme (−13.1 eV), where the oxygen atomic energies are raised significantly, the 12 highest occupied levels are shifted upward so as to lower the HOMO – LUMO gap from 4.4 to 3.0 eV. Most of the displaced molecular orbitals also involve mixtures of atomic p orbitals from the chain oxygens, but now there is some occasional d(π)–p(π) bonding character with titanium (Figure 5b).

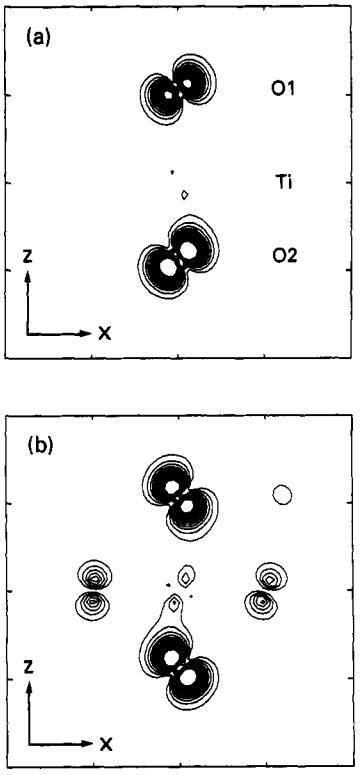

Figure 5. Electron density for selected molecular orbitals, viewed in the xz plane. Each plot is contained within an 8 Å × 8 Å square, with Ti of group 0 at the center and O1 and O2 above and below, respectively. Contours are evenly spaced over the lower half of the surface. (a) Orbital 19; $H_{ii} = -19.8$ eV. Charge is transferred from the titanium to the chain oxygens, which have been deliberately made more electronegative. This orbital is one of the lowermost group of 12 at the left in Figure 4b. (b) Orbital 53; $H_{ii} = -13.1$ eV. From the highest-lying group of 12 occupied orbitals at the right in Figure 4b.

Second Harmonic Generation

The wavelength of the incident light is taken as 1064 nm, with the β tensor given in units of 10^{-30} cgs throughout. All singly-excited states of $[TiO_5\text{--}TiO_6\text{--}TiO_5]^{20-}$ have been generated from the subset of orbitals illustrated in Figure 4. The central TiO_6 octahedron in each structure contains a long Ti--O bond of 2.15 Å, a short bond of 1.74 Å, and an intermediate bond of 1.99 Å, as described above. The hyperpolarizabilities computed in the various examples are understood to be local to this central grouping, which for ease of reference we will denote as group 0. The TiO_6 clusters sharing O1 and O2 will be referred to as groups 1 and −1, respectively.

Molecular orbitals for the various structures were determined initially in the coordinate system of Figure 2. The origin of each set of coordinates was then shifted to the appropriate electronic charge centroid for calculation of the hyperpolarizabilities. Thus any given β has been computed in a reference frame in which the electronic contribution to the ground state dipole moment of the full trimer is zero.

Variation of the Ti--O--Ti Angle. Figure 6 displays β_{ijk} versus θ for all unique tensor components, although

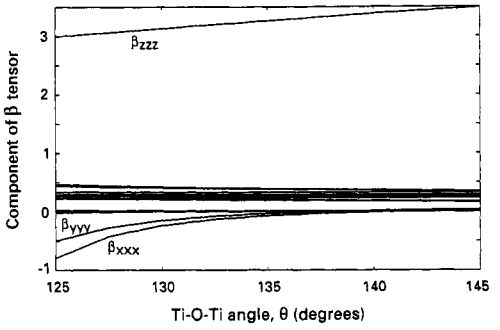

Figure 6. Point-to-point plots of the local SHG components, β_{ijk}, versus θ. Units are 10^{-30} cgs, and the incident wavelength is 1064 nm. Only those tensor components that vary significantly over the range of θ are labeled explicitly.

only those components that vary appreciably with the Ti--O--Ti angle (namely β_{xxx}, β_{yyy}, and β_{zzz}) are labeled explicitly on the diagram. The largest component is β_{zzz}, which corresponds to both incident and second harmonic radiation polarized along the asymmetric O1--Ti--O2 axis of group 0. This particular component, β_{zzz}, is responsible for most of the θ dependence in the nonlinear response as well, increasing by approximately 15% between $\theta = 125°$ and $\theta = 145°$. The perpendicular components β_{xxx} and β_{yyy} are nearly zero and roughly constant for $\theta \geq 135°$. β_{xxx} and β_{yyy} acquire more substantial magnitude at lower angles, however, as groups 1 and −1 begin to bend further away from the vertical. We emphasize again that these local hyperpolarizabilities do not arise merely from the

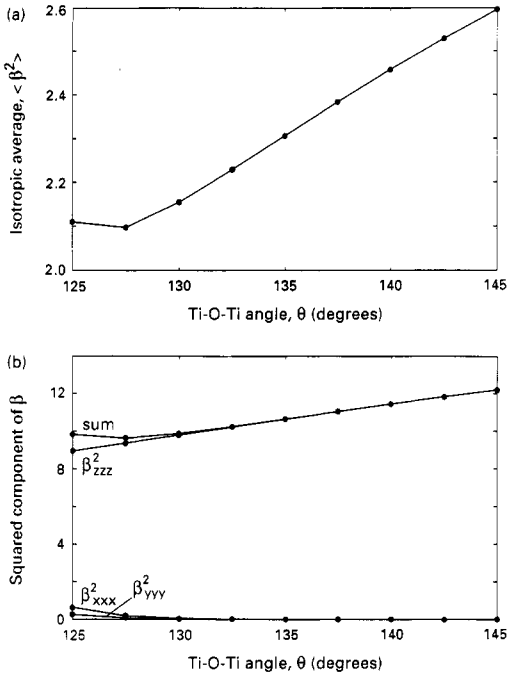

Figure 7. (a) Variation of the isotropically averaged SHG tensor, $\langle\beta^2\rangle$, with Ti--O--Ti angle. (b) Sum of the squared components β_{xxx}^2, β_{yyy}^2, and β_{zzz}^2, taken as an approximation to $\langle\beta^2\rangle$. Polarizations perpendicular to the O1--Ti--O2 direction become more important as θ decreases.

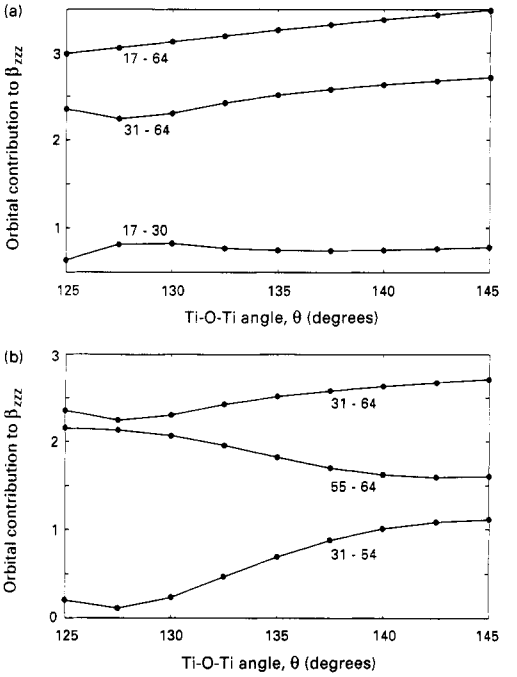

Figure 8. Variation of tensor component β_{zzz} with θ. (a) Subdivided into two- and three-state contributions originating from bonding orbitals (17–30) and nonbonding orbitals (31–64). The full values are shown in the upper curve, labeled 17–64. (b) Contribution attributable only to nonbonding orbitals (31–64), divided arbitrarily into lower (31–54) and upper (55–64) groups.

tensor transformation (A3); rather, the changes in the SHG tensor reflect the altered electronic distribution about the *fixed* nuclei of the central TiO_6.

To facilitate comparison with powder SHG measurements, in Figure 7a we plot the isotropic average $\langle\beta^2\rangle$ given in eqs A1 and A2. Except for a very slight decrease in going from $\theta = 125°$ to $\theta = 127.5°$, the general tendency again is for an increase in SHG efficiency as the Ti--O--Ti angle increases. The values of $\langle\beta^2\rangle$ at the lowest angles are also attributable to growing influence from the perpendicular components, as is made clear in Figure 7b. A simple comparison of the individual quantities β_{xxx}^2, β_{yyy}^2, and β_{zzz}^2 to the sum $\beta_{xxx}^2 + \beta_{yyy}^2 + \beta_{zzz}^2$ demonstrates the relative importance of $\langle\beta_{xxx}^2\rangle$ and $\langle\beta_{yyy}^2\rangle$ at lower θ. Note that, in making the comparison in Figure 7b, we neglect all but the first summation in each of eqs A2a, A2b, and A2c—a good approximation given the constancy of the remaining components. Overall, $\langle\beta^2\rangle$ increases by nearly 25% over the range of angles considered.

Let us undertake next a subdivision of β_{zzz} into contributions associated with different molecular orbitals. Each singly-excited state in the extended Hückel model, $|n\rangle = |a \rightarrow u\rangle$, is formed by promoting an electron from an occupied molecular orbital $|a\rangle$ to an unoccupied orbital $|u\rangle$. A given diagonal (or two-state) term $\langle g|\hat{Z}|n\rangle\langle n|\hat{Z}|n\rangle\langle n|\hat{Z}|g\rangle$ therefore "originates" from a single molecular orbital $|a\rangle$, whereas every off-diagonal (or three-state) term $\langle g|\hat{Z}|n\rangle\langle n|\hat{Z}|m\rangle\langle m|\hat{Z}|g\rangle$ is determined by two orbitals, $|a\rangle$ and $|b\rangle$, the latter function defining the excited state $|m\rangle = |b \rightarrow v\rangle$. For each component in the sum-over-states expression (2), we then either credit its full value to $|a\rangle$ or split the contribution equally between $|a\rangle$ and $|b\rangle$, depending on whether the matrix element is diagonal or off-diagonal. Such a partitioning of β_{zzz} gives one a rough idea of how various classes of excitation formally contribute to the nonlinear optical response.

Figure 8a sets out the angular variation of β_{zzz} as allotted to two broad categories of origination orbital $|a\rangle$: bonding (17–30) and nonbonding (31–64). We have described these orbitals in some detail in previous work, and have discussed their role in determining β_{zzz} when long and short Ti--O bonds are varied in a TiO_6 trimer with θ constant at 135°. There it was demonstrated that orbitals over the entire range, bonding as well as nonbonding, contribute significantly to the hyperpolarizability of fixed monomeric and trimeric structures.[4] Now, with the Ti--O--Ti angle allowed to vary, we observe that the $n \rightarrow \pi^*$ transitions account for almost the entire sensitivity of β_{zzz} to θ. Contributions attributable to the bonding orbitals remain roughly constant at approximately 30% those of the nonbonding orbitals, while values from the latter group increase monotonically for θ greater than 127.5°.

Lumped together under the generic classification of "nonbonding" are many specific combinations, however, and the nonlinear response within this large group is hardly uniform. A given nonbonding orbital will generally involve some mixture of oxygen p orbitals associated with one or more TiO_6 groups, directed along various axes with either π or σ overlap. Orbital character is hard to classify owing to the low symmetry of the complete structure. Aside from the very general separation into bonding and nonbonding contributions made in Figure 8a, we see little point in making any finer distinctions. What is important, though, is that no single nonbonding orbital emerges as being of singular importance in establishing β_{zzz}—not even the highest occupied levels, as is sometimes asserted on general grounds for smaller and simpler systems. In these TiO_6 trimers, at least, each of the nonbonding orbitals helps uniquely to determine the variation of β_{zzz} with θ. Some individual contributions go up and some go down as the angle changes; some are constant at smaller angles while others remain constant at larger angles. Still others

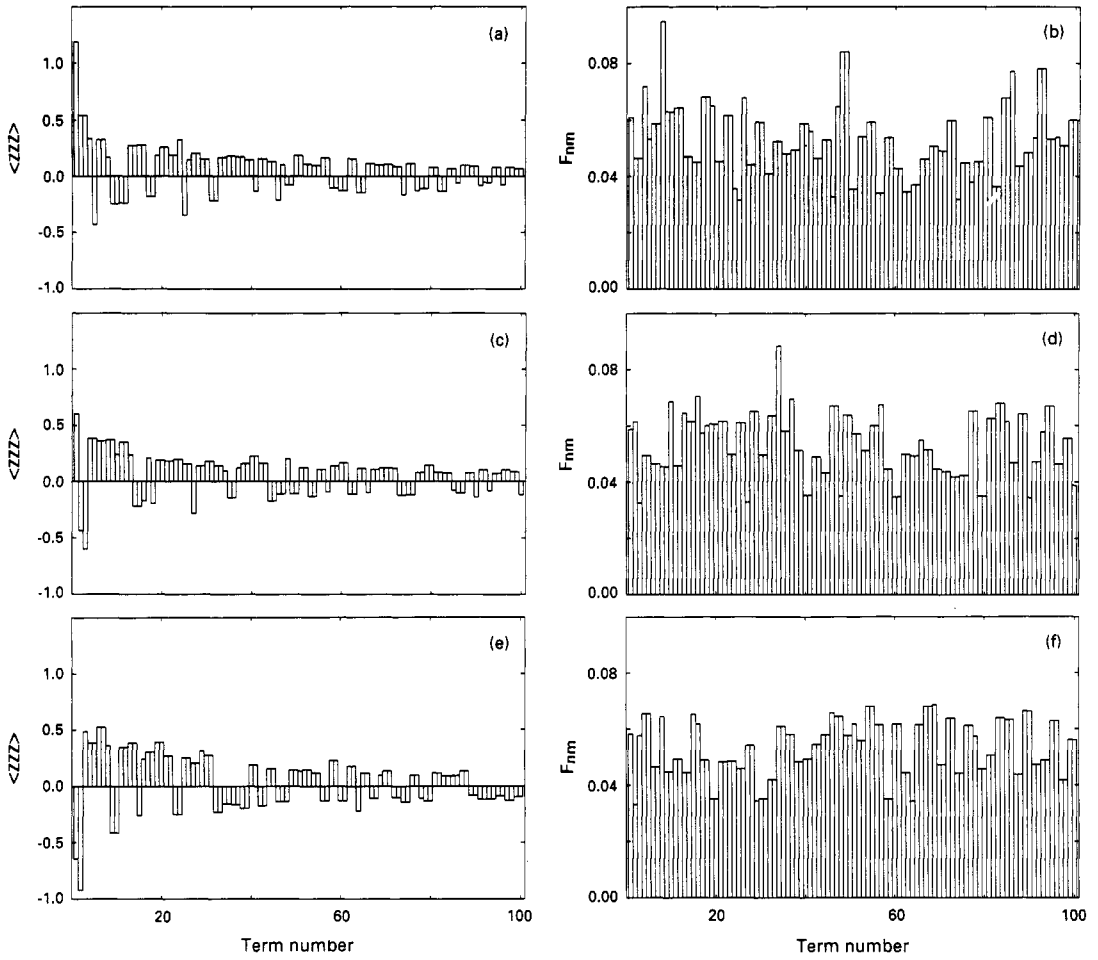

Figure 9. Matrix elements $\langle zzz \rangle$ (left-hand column) and associated energy factors F_{nm} (right-hand column) for the 100 largest terms in the sum over states. The complete terms b_{nm} are numbered in order of descending absolute value. H_{ii} = −14.8 eV. (a), (b) θ = 125°; (c), (d) θ = 135°; (e), (f) θ = 145°.

vary little at all. To illustrate this point, in Figure 8b we show an arbitrary breakdown of the nonbonding contributions into a lower group (31–54) and an upper group (55–64). Here the two curves demonstrate opposing tendencies, and the net increase in β_{zzz} arises as a small difference between large terms. Such cancellations are a recurring theme in the formal analysis of sum-over-states expressions for Ti--O model systems.

Partial cancellation of terms, arising in particular from alternation of the algebraic sign in the sum over states, is brought out clearly by the additional breakdown of β_{zzz} in Figure 9. For this display the perturbative expression is simplified to

$$\beta_{zzz}(\omega) = \sum_{n,m} b_{nm}(\omega) \tag{7}$$

where

$$b_{nm}(\omega) = KF_{nm}(\omega)\langle zzz \rangle \tag{8}$$

The factor $F_{nm}(\omega)$ is a function of the energy factors f defined in (4), and $\langle zzz \rangle$ is the matrix element $\langle g|\hat{Z}|n\rangle\langle n|\hat{Z}|m\rangle\langle m|\hat{Z}|g\rangle$ defined in (3). Various physical constants are taken up in the proportionality constant K. The terms b_{nm} are then arranged in order of descending magnitude, without regard to sign, so that we obtain a rank-ordered list of the contributions made by each pair of excited states. In Figure 9 the top 100 terms are selected and separated further into their component factors $\langle zzz \rangle$ and F_{nm}, with the matrix elements at the left and the corresponding energy factors at the right. Results are shown (from top to bottom) for θ = 125°, θ = 135°, and θ = 145°.

Figure 9 makes clear that no single virtual transition dominates the sum over states. Most of the matrix elements are of similar magnitude, and there are frequent changes in sign. When θ is equal to either 125° or 135°, for example, roughly 30 matrix elements of the 100 are negative. The net change in β observed over the range of Ti--O--Ti angles is simply too small to trace at this level of detail. Nor can the change be ascribed to the energy factors, which in each case maintain a relatively flat distribution at nearly the same average level.

The constancy of the energy factors does suggest, though, that another approach might be provided by the Unsöld approximation (6), which links the nonlinear response to the third moment of the ground-state electron distribution. Figure 10 shows, as a first step, the difference in total electron density between a structure with θ = 145° and one with θ = 125°. The density difference is represented both as a surface and as a contour plot and is computed over an 8 Å × 8 Å square with the titanium of group 0 at the origin. Positive regions on the surface correspond to increased electron density in the system with larger θ; negative regions (shown as broken contours in the diagram below) correspond to an outflow of electrons as the angle is increased. Aside from the trivial displacement of charge associated with the physical movement of the oxygens in groups 1 and −1, the principal change is a small increase of density in the region between O1 and the titanium of

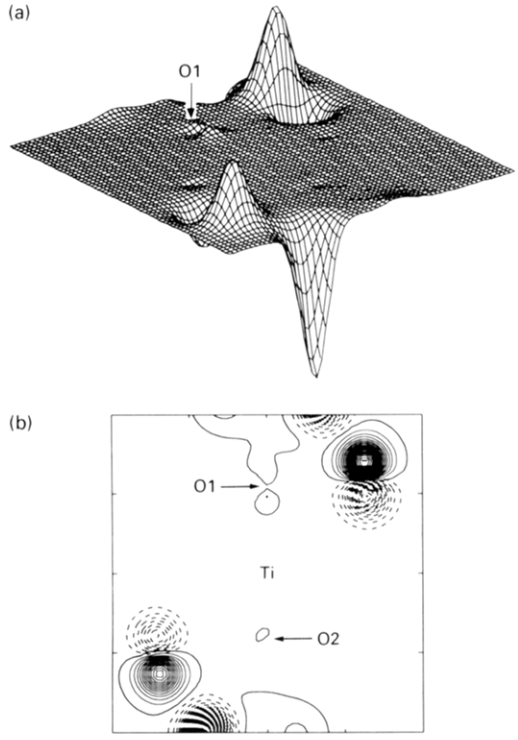

Figure 10. Difference in total electron density between a structure with $\theta = 145°$ and one with $\theta = 125°$, taken in the xz plane. The net change in the central TiO_6 group is a barely perceptible shift of charge toward O1. (a) Surface plot, 8 Å × 8 Å. Positive regions correspond to a relative gain of electrons by the system with $\theta = 145°$. The most pronounced features simply reflect the displacement of oxygens in groups 1 and −1. (b) Evenly spaced contour plot with levels ranging from −0.8 to 0.5; 8 Å × 8 Å. Positive contours are indicated by solid lines; negative contours by broken lines.

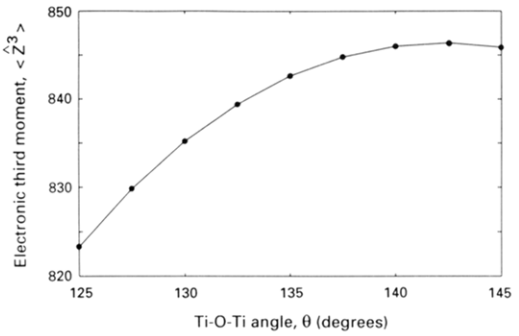

Figure 11. Electronic third moment $\langle \hat{Z}^3 \rangle$, in atomic units, versus θ. The moments are computed in a coordinate system where the ground-state electronic dipole moment is zero.

the adjacent group 1. Note that, for each value of θ, this particular oxygen is 2.15 Å away from Ti(0) but 1.74 Å from Ti(1). O2, by contrast, remains 1.74 Å away from Ti(0) but 1.99 Å from Ti(−1). The result of bending the structure over a range of 20° is thus to concentrate a small amount of additional charge between O1 and Ti(1), and it is this minor redistribution that is presumably relevant to the local hyperpolarizability. Indeed, a plot of $\langle \hat{Z}^3 \rangle$ vs θ in Figure 11 demonstrates that the Unsöld estimates loosely track the values of β_{zzz} computed using the full sum-over-states expression. The third moment (local to group 0) increases slowly but steadily over the range $125° \leq \theta \leq 135°$ before reaching a plateau at higher values of θ. The change in the third moment develops in response to the slight additional asymmetry introduced by the preferential shift of charge to the O1--Ti(1) bond.

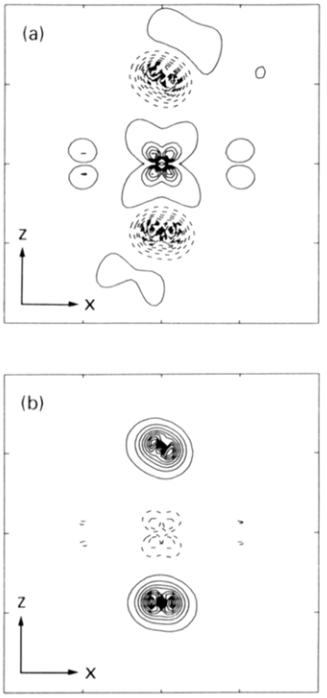

Figure 12. Changes in total electron density brought about by varying the Hückel parameter H_{ii} for the chain oxygens (Figure 3b). Contours in the xz plane (levels ranging from −0.11 to 0.13) indicate differences relative to densities computed with the standard value $H_{ii} = -14.8$ eV. (a) Decreased ionization potential; $H_{ii} = -13.1$ eV. (b) Increased ionization potential; $H_{ii} = -16.8$ eV. Conventions are as in Figures 5 and 10.

Variation of Oxygen Electronegativity. Here we explore how the computed hyperpolarizability is affected by deliberate changes in the Hückel parameters for the chain oxygens (as marked in Figure 3b). Fixing θ at 135°, we vary H_{ii} for the 2p orbitals above and below the standard value of −14.8 eV. More negative values effectively increase the orbital ionization energy and thereby make the oxygen more electronegative; by similar reasoning, more positive values of H_{ii} reduce the ionization energy and consequently make the oxygen more electropositive. Overall effects on the energy levels have already been illustrated in Figure 4b, and now in Figure 12 we show the gross changes in the electron distribution for structures with $H_{ii} = -13.1$ and −16.8 eV. The contours, which in each example represent differences in total electron density relative to a standard system with $H_{ii} = -14.8$ eV, demonstrate how electrons can be made to flow either toward or away from the oxygens.

Figure 13 shows the value of $\langle \beta^2 \rangle$ determined over a wide range of H_{ii}. Nonlinear response is quenched almost entirely as H_{ii} approaches −20 eV, by which point electron density is withdrawn significantly from the titanium. $\langle \beta^2 \rangle$ then rises steadily as the ionization potential is lowered, and reaches a maximum near −13.1 eV. Past this value of H_{ii}, however, the perturbative expression is dominated by the energy factors (4), which suddenly become large and resonant and which therefore make the sum-over-states results unreliable. Over the relatively narrow range of 14.8 ± 1 eV, $\langle \beta^2 \rangle$ varies by approximately a factor of 3.

To trace the source of these changes, we display in Figure 14 the distribution of β_{zzz} over various orbitals of origination (similar to the analysis in Figure 9). Plotted on the same scale, the distributions for $H_{ii} = -19.8$, −14.8, and −13.1 eV reveal striking differences among the three

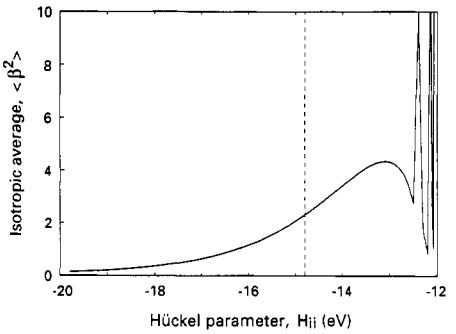

Figure 13. Variation of the isotropically averaged SHG tensor, $\langle\beta^2\rangle$, with H_{ii}. $\theta = 135°$. The dashed vertical line indicates the reference value $H_{ii} = -14.8$ eV. Values plotted to the right of the maximum near $H_{ii} = -13.1$ eV are inaccurate owing to resonances in the sum-over-states expression.

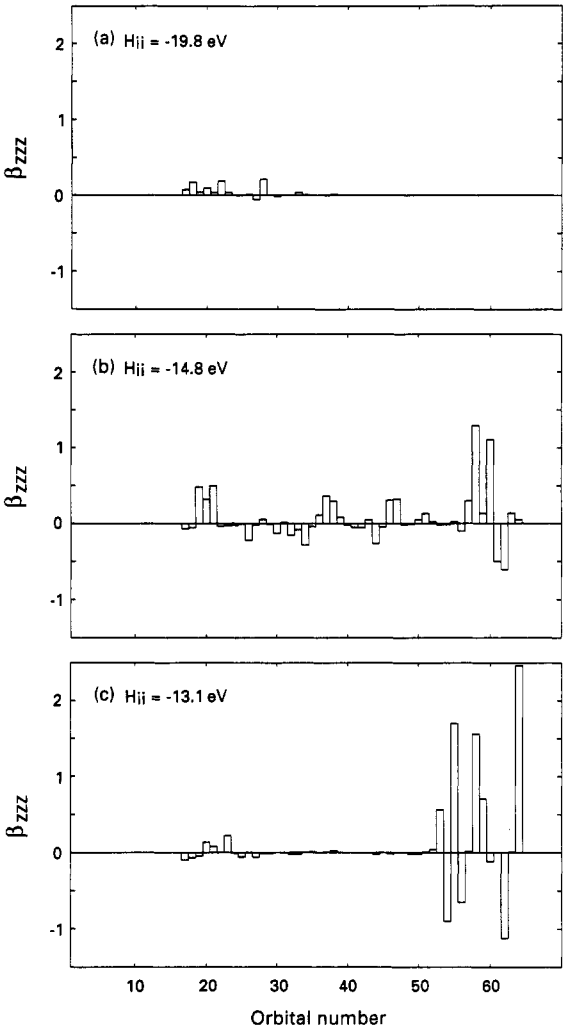

Figure 14. Breakdown of β_{zzz} into specific contributions from the occupied orbitals. Each bar represents the amount attributable to all virtual transitions originating from the designated level. $\theta = 135°$. (a) $H_{ii} = -19.8$ eV; (b) $H_{ii} = -14.8$ eV; (c) $H_{ii} = -13.1$ eV.

systems. In the standard case, contributions to β_{zzz} originate from the whole range of occupied orbitals, with just over 75% coming from the nonbonding orbitals (31–64). When, on the other hand, the Hückel parameter is very negative, what little hyperpolarizability there is comes almost entirely from orbitals 17 through 28. This group contains the localized oxygen-like combinations that lie 5 eV below the main group of bonding orbitals, and accounts for nearly 95% of β_{zzz}. The relevant levels have already been illustrated in the left panel of Figure 4b, and a representative orbital density has been shown in Figure 5a. In the third example of Figure 14, where H_{ii} is least negative, 98% of the enhanced hyperpolarizability arises from the 12 highest occupied orbitals. This group, too, coincides with a family that moves away from the main band, as has been noted in the rightmost panel of Figure 4b. The levels are shifted upward in response to the increased energies of the oxygen 2p atomic orbitals.

Having identified the specific levels involved in the nonlinear optical response, we can now disentangle the energy factors F_{nm} from the matrix elements $\langle zzz\rangle$ in (7) and (8). Distributions of F_{nm} and $\langle zzz\rangle$ for the 100 b_{nm} of largest magnitude are shown in Figure 15. Although individual $\langle zzz\rangle$ matrix elements are somewhat larger when $H_{ii} = -13.1$ eV, both the basic shape of the distribution and its pattern of alternation between positive and negative terms remain common to all three systems. Moreover, the magnitude of the local electronic third moment, $\langle\hat{2}^3\rangle$, changes much more slowly than does β_{zzz} over the range $-19.8\text{ eV} \le H_{ii} \le -13.1$ eV, in fact decreasing by about 10% while β_{zzz} itself increases approximately 5-fold. But, as is clear from the right-hand column of Figure 15, the energy factors increase by nearly an order of magnitude over the same range. Thus the enhancement of β derives predominantly from more favorable excited-state energies, which in turn trace back to the shifts of the individual molecular orbitals.

In concluding this analysis, we should note that β is affected similarly by changes in the Hückel parameters for the oxygens *outside* the --Ti--O--Ti--O-- chain. With H_{ii} for the chain oxygens fixed at −14.8 eV, for example, $\langle\beta^2\rangle$ increases from 1.81 to 5.12 as H_{ii} for all the other oxygens is varied from −17.8 to −12.8 eV. Apparently it is the ability of either class of oxygen to shift in energy while bringing about a transfer of charge to or from the titanium that is most significant. We will speculate briefly on the experimental implications of these results in the following section.

Review of Experimental Measurements

Efforts to link the observed variation in powder SHG efficiency with changes in crystal structure for a number of KTP isomorphs have yielded an apparent correlation between the chain Ti--O--Ti angle and the powder ensemble average $\langle\beta^2\rangle$. Note that the geometries of the TiO_6 octahedra change very little in the systems $K_{1-x}Na_xTiOPO_4$, $KTiOP_{1-x}As_xO_4$, $K_{1-x}Na_xTiOAsO_4$, and $K_{1-x}Ag_xTiOPO_4$; the long and short Ti--O bond alternation is retained along the --Ti--O--Ti--O-- chain, and the equatorial Ti--O bonds maintain their average values. No feature of an individual TiO_6 octahedron can thus account for the observed variation in SHG performance. The angles in the Ti--O chains do change slightly, though, as either the unit cell expands or contracts to accomodate ions of different sizes or as the chain oxygens alter their coordination with the monovalent exchange cations. In the $KTiOP_{1-x}As_xO_4$ system, for example, the powder SHG signal increases by 17% in going from $x = 0$ to $x = 1$ while, at the same time, the average Ti--O--Ti angle increases by 5.5°.[37] In the system $K_{1-x}Na_xTiOPO_4$ it was originally reported that the powder SHG signal is almost unchanged between $x = 0$ (average $\theta = 134.2°$) and $x = 0.5$ ($\theta = 132.5°$)

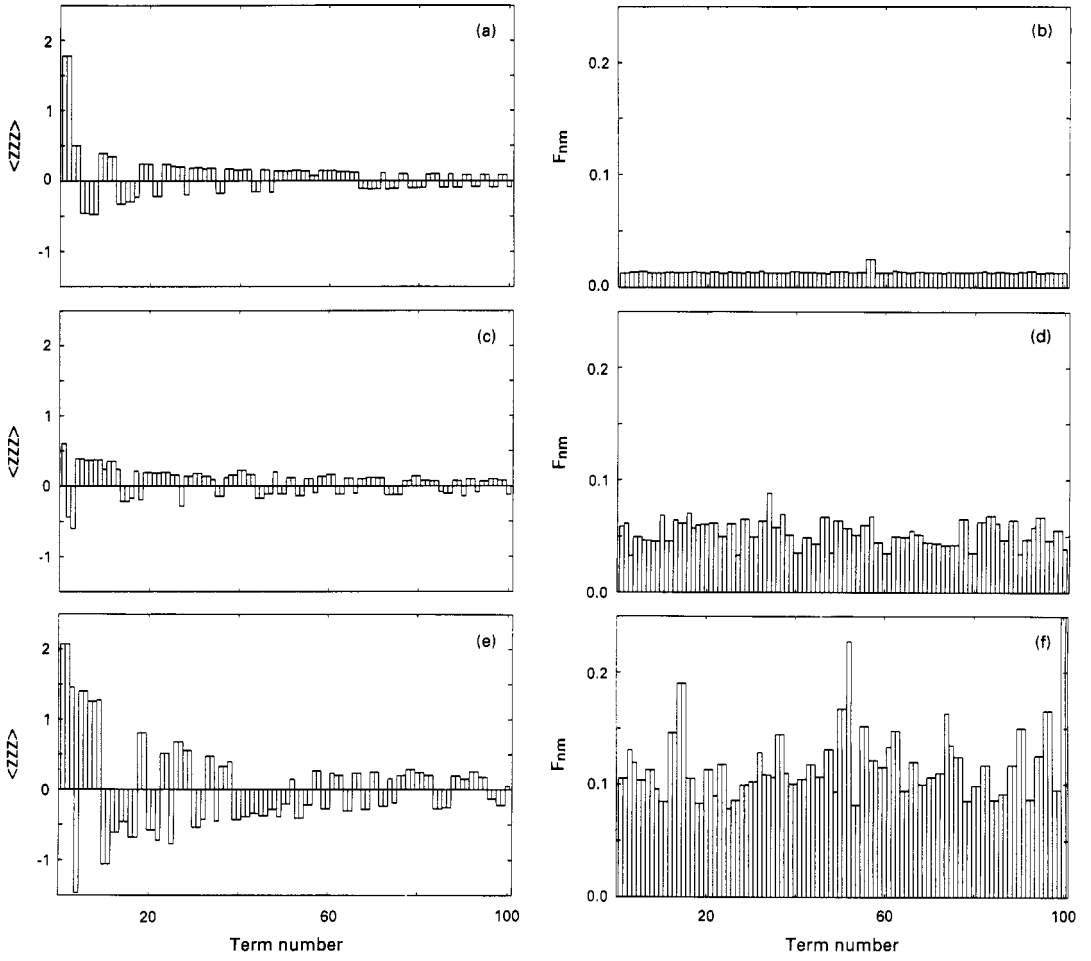

Figure 15. Matrix elements $\langle zzz \rangle$ (left-hand column) and energy factors F_{nm} (right-hand column) for the 100 largest terms in the sum over states. The complete terms b_{nm} are numbered in order of descending absolute value. $\theta = 135°$. (a), (b) $H_{ii} = -19.8$ eV; (c), (d) $H_{ii} = -14.8$ eV; (e), (f) $H_{ii} = -13.1$ eV (the last term in 15f is off scale at $F_{nm} = 0.42$.)

but then falls by an order of magnitude as x approaches 1 ($\theta = 131.6°$).[16] Our own measurements on this material reveal a similar trend, although the overall drop in $\langle \beta^2 \rangle$ across the full range of composition is only 30%, with the intensity relative to KTP going from 0.81 ($x = 0.5$) to 0.68 ($x = 1$). There is a concomitant decrease in the Ti--O--Ti angle as K is replaced by Na. These results, and those for other isomorphs such as $AgTiOPO_4$ and $NaTiOAsO_4$,[18] are broadly consistent with predictions from the theoretical calculations above.

There is also a correlation between the Ti--O--Ti angle and the electronegativity of the substituent cations, although changes in the angle may have different origins depending on whether the site of substitution is within the framework (phosphorus atom) or is outside the framework (potassium atom). This consideration means that the two effects we have described—namely, the variation of $\langle \beta^2 \rangle$ with both the Ti--O--Ti angle and with the ionization potential of the chain oxygens—act cooperatively and hence cannot be examined separately in real systems. We might then expect to observe a change in $\langle \beta^2 \rangle$ larger than that predicted from either of the calculations taken in isolation.

At this point, let us consider how the model in which H_{ii} for the chain oxygens is varied over a wide range of energy may be related to the real chemical systems involving cation substitution. We examine the --Ti--O--Ti--O-- chain in isolation from the rest of the KTP structure initially. Increasing the electronegativity of the oxygens (making H_{ii} more negative) causes these atoms to gain electrons, thereby leaving the titanium more positive. Conversely, reducing the electronegativity causes charge to build up on the titanium at the expense of the oxygen.

The results above show that, in the case of increased oxygen electronegativity, $\langle \beta^2 \rangle$ is reduced primarily because of the much smaller energy factors which result from the principal orbitals being sharply lowered in energy. We suggest that any substitution of cations in the KTP structure capable of altering the electron density in the Ti--O chains will cause changes in β similar to those we have computed by adjusting H_{ii}. Replacement of the external potassium ion by a more electronegative species such as sodium, for example, will tend to draw electron density out of the conjugated Ti--O--Ti--O chain and thus concentrate more of the remaining charge on the chain oxygens. This redistribution is tantamount to lowering the electronegativity of the oxygens, and consequently the oxygen orbitals will be effectively lowered relative to the titanium and $\langle \beta^2 \rangle$ will be lowered. Conversely, if a less electronegative ion is inserted, more electrons will be

(37) The original relative merit of KTA determined by phase-matched single-crystal SHG indicated a 60% improvement in the nonlinear optical coefficients.[38] Recent measurements, however, have caused this result to be revised so that the single-crystal value is now in close agreement with the powder SHG value.[39]

(38) Bierlein, J. D.; Vanherzeele, H.; Ballman, A. A. *Appl. Phys. Lett.* **1989**, *54*, 783.

(39) Cheng, L. T. A.; Cheng, K. L. K.; Bierlein, J. D.; Zumsteg, F. C. *Proc. SPIE*, in press.

available to the entire chain. The density around the oxygens will then be reduced relative to the titanium and the associated orbital energies raised correspondingly. In our simple model, the former case is equivalent to lowering H_{ii} and the latter is equivalent to raising it.

While remaining aware of these general features, we must nevertheless refrain from overinterpreting the model calculation. What the graph in Figure 13 shows is merely the variation of $\langle\beta^2\rangle$ over the full range of the parameter H_{ii}. No suggestion is made that the points correspond to identifiable systems, or even that chemical substitution can bring about electron-withdrawing effects of this magnitude. Yet one does learn how and why the nonlinear response computed at the extended Hückel level is sensitive to oxygen electronegativity, and from this perspective one can draw certain parallels with the experimental data.

Summary

We have computed the nonlinear optical response of an octahedrally distorted TiO_6 group on the basis of extended Hückel wavefunctions and a perturbative sum-over-states formalism. The TiO_6, viewed as an integrated component of a trimeric [TiO_5--TiO_6--TiO_5] chain, is used as a simple, idealized model of the KTP system.

Isotropic averages of the squared hyperpolarizability tensor, $\langle\beta^2\rangle$, which should be proportional to SHG powder intensity, increase by 25% as the Ti--O--Ti angle in the chain goes from 125° to 145°. Most of the increase is taken up by the β_{zzz} component in a coordinate system where z is the C_4 axis of the distorted octahedron. This relatively modest, although certainly measurable, enhancement of the nonlinear response follows from the perturbed local electronic structure at the different angles, as reflected by changes in the electronic third moment. The variation in local hyperpolarizability is intrinsic to the system and not merely a measure of the angular transformation properties of the tensor. These results are consistent with the correlation between SHG efficiency and Ti--O--Ti angle that has been observed experimentally for the KTP isomorphs.

For unperturbed systems, contributions to the sum over states are distributed over the entire range of occupied orbitals. Increasing the electronegativity of the oxygens relative to the titanium, however, results in the formation of localized oxygen orbitals at lower energies. Most of the terms in the sum then originate from these perturbed levels, and second harmonic generation in the model system is reduced as a result. When, by contrast, the oxygen electronegativity is decreased, the energies of the uppermost oxygen orbitals are raised so that the nonlinear response enjoys a significant near-resonant enhancement.

Acknowledgment. We thank S. J. Crennell and R. J. Thrash for providing the powder SHG test data on the KNaTP series.

Appendix

Powder SHG intensity is proportional to the isotropic quantity

$$\langle\beta^2\rangle = \langle\beta_{FFF}{}^2\rangle + \langle\beta_{FGG}{}^2\rangle + \langle\beta_{FGH}{}^2\rangle \tag{A1}$$

where the three terms on the right-hand side are given by

$$\langle\beta_{FFF}{}^2\rangle = {}^1/_7\sum_i \beta_{iii}{}^2 + {}^6/_{35}\sum_{i\neq j}\beta_{iii}\beta_{ijj} + {}^9/_{35}\sum_{i\neq j}\beta_{iij}{}^2 + {}^6/_{35}\sum_{\substack{ijk\\ \text{cyclic}}}\beta_{iij}\beta_{jkk} + {}^{12}/_{35}\beta_{ijk}{}^2 \tag{A2a}$$

$$\langle\beta_{FGG}{}^2\rangle = {}^1/_{35}\sum_i \beta_{iii}{}^2 - {}^2/_{105}\sum_{i\neq j}\beta_{iii}\beta_{ijj} + {}^{11}/_{105}\sum_{i\neq j}\beta_{iij}{}^2 - {}^2/_{105}\sum_{\substack{ijk\\ \text{cyclic}}}\beta_{iij}\beta_{jkk} + {}^8/_{35}\beta_{ijk}{}^2 \tag{A2b}$$

$$\langle\beta_{FGH}{}^2\rangle = {}^1/_{105}\sum_i \beta_{iii}{}^2 - {}^1/_{35}\sum_{i\neq j}\beta_{iii}\beta_{ijj} + {}^2/_{35}\sum_{i\neq j}\beta_{iij}{}^2 - {}^1/_{35}\sum_{\substack{ijk\\ \text{cyclic}}}\beta_{iij}\beta_{jkk} + {}^1/_7\beta_{ijk}{}^2 \tag{A2c}$$

with the summation indexes as follows:

$$i \rightarrow x, y, z$$
$$i \neq j \rightarrow xy, xz, yx, yz, zx, zy$$
$$ijk, \text{cyclic} \rightarrow xyz, yzx, zxy$$

These results derive from the fundamental transformation of a third-rank tensor from a molecule-fixed coordinate system (ijk) to a laboratory frame (FGH), for which the two reference frames are related by a set of direction cosines a:

$$\beta_{FGH} = \sum_{ijk} a_{Fi}a_{Gj}a_{Hk}\beta_{ijk} \tag{A3}$$

Averaging over all angular orientations yields the quantities given above, as has been shown by Cyvin et al.[34]